Available online at www.sciencedirect.com
SCIENCE DIRECT
Polymer 47 (2006) 5852–5861
polymer
www.elsevier.com/locate/polymer

# Plastic deformation and damage of polyoxymethylene in the large strain range at elevated temperatures

J. Mohanraj [a], D.C. Barton [a], I.M. Ward [b,*], A. Dahoun [c], J.M. Hiver [c], C. G'Sell [c]

[a] School of Mechanical Engineering, University of Leeds, Leeds LS2 9JT, UK
[b] IRC in Polymer Science and Technology, School of Physics and Astronomy, University of Leeds, Leeds LS2 9JT, UK
[c] Ecole des Mines de Nancy, INPL, Parc de Saurupt, 54042 Nancy, France

Received 22 March 2006; received in revised form 5 June 2006; accepted 6 June 2006
Available online 30 June 2006

**Abstract**

The deformation behaviour of polyoxymethylene has been studied in plane strain compression at temperatures from 120 °C up to 165 °C and in uniaxial tension and simple shear at 160 °C for strain rates from $10^{-4}$ to 1 $s^{-1}$. In uniaxial tension the stress–strain behaviour was determined by a novel video-controlled testing system. The measurements showed that there was a very significant evolution of volumetric strain, indicating that damage mechanisms play a key role in the plastic deformation behaviour.

All tests showed similar deformation stages with a short region of visco-elastic behaviour followed by a rounded yield point. The von Mises equivalent yield stress for these tests showed a linear relationship with logarithmic strain rate, suggestive of an Eyring type thermally activated process. After yielding, all stress–strain curves showed a long plastic deformation regime, which in shear occurred at constant stress. In plane strain compression there was also only a very small increase in stress, in contrast to uniaxial tension where very significant strain hardening was observed at high strains, which is attributed to the onset of structural changes.


*Keywords:* Polyoxymethylene; Plastic deformation; Damage

## 1. Introduction

Substantial improvement in properties as a result of molecular orientation has initiated the development of several thermoforming processes to orient semi-crystalline polymers [1]. These processes include die-drawing [2–5], hydrostatic extrusion [2,6,7], rolling [8,9], roll-drawing [10], constrained rolling [11,12], etc. These processes have been developed in the last five decades for producing polymeric products of significant length (sheets, tubes, rods or filaments) with higher modulus and strength. In this important research effort to develop efficient orientation techniques, the Leeds group has made a major contribution, particularly in relation to hydrostatic extrusion and die-drawing processes.

Among the variety of polymers investigated, polyoxymethylene – POM for short – appeared as a serious candidate for solid-state forming [5]. This choice was motivated by several related reasons: (i) the flexible chains, with their $-CH_2-O-$ monomers, allow helical configuration and facilitate crystallisation, (ii) the mechanical properties at room temperature ($E = 3.1$ GPa and $\sigma_y = 72$ MPa) are already good in the non-oriented state, (iii) the working range between glass transition ($T_g = -75$ °C) and melting point ($T_m = 178$ °C) is quite extended, (iv) the friction coefficient against steel ($\mu = 0.075$) is low enough for easy polymer sliding against the forming tools [13], and (v) in the oriented state, the retention of mechanical properties is good at fairly high temperatures ($T_{max} \approx 165$ °C).

However, the development of a forming process requires robust control of the operational parameters. In this respect, experimentation on laboratory apparatus or industry pilot units

* Corresponding author. Tel.: +44 113 3433808; fax: +44 113 3433846.
*E-mail address:* i.m.ward@leeds.ac.uk (I.M. Ward).

0032-3861/$ - see front matter © 2006 Elsevier Ltd. All rights reserved.
doi:10.1016/j.polymer.2006.06.008

is of limited value. Computer simulations are therefore needed for optimising the thermoforming processes efficiently. However, despite serious efforts to develop numerical models [14], quantitative predictions are inaccurate because the constitutive equations of the materials are unknown or insufficiently defined. The deformation behaviour of polymers is very sensitive to temperature, strain, strain rate and hydrostatic pressure. It is thus critical to investigate their response in more detail at large strains under various loading conditions.

Plastic deformation of semi-crystalline polymers involves a multitude of microstructural and morphological transformations that are activated in both the crystalline and amorphous domains. Following the pioneering work of Peterlin [15], many authors have studied the elementary mechanisms that control macroscopic deformation: viscous flow of entangled macromolecules, chain slip in the crystalline lamellae, crystal tilt and twinning, phase transformation, etc. (e.g. [16]). These authors have pointed out the dramatic microstructural evolution from isotropic spherulites to highly oriented microfibrils.

To model quantitatively the deformation of semi-crystalline polymers, it has been assumed initially that their deformation kinetics was controlled by the stress deviator only, so that their generalised plastic behaviour could be modelled by the classical von Mises laws prevailing in mechanical metallurgy. In other words, it was supposed that the von Mises ''equivalent'' stress–strain equation, $\sigma_{eq}(\varepsilon_{eq}, \dot{\varepsilon}_{eq})$, is intrinsic for the polymer at a given temperature, and that the response under any arbitrary strain path can be deduced from simple tensile tests. It is interesting to note that this scheme is still evoked in most finite-element codes utilised for predicting plastic deformation of polymeric structures. However, this first approximation is not fully satisfactory for polymers because specific phenomena violate the simple flow rules.

The first effect to be taken into account is the influence of hydrostatic stress, $\sigma_H = 1/3(\sigma_{11} + \sigma_{22} + \sigma_{33})$, on the measured flow stress [17–19]. This leads to the conclusion that plastic deformation in uniaxial tension is relatively easier than in specific processes involving high pressures, such as hydrostatic extrusion [6]. Consequently, the usual deviatoric criteria that have been adopted as a first approximation by many authors (e.g. [14,20]) for the die-drawing process should in general be replaced by a more realistic criterion taking into account explicitly the effect of the hydrostatic component of stress.

Another important problem to be taken into consideration is the anisotropy due to the development of orientation textures in solid polymers subjected to plastic deformation under various deformation modes. This has been unambiguously demonstrated and modelled by several authors [21,22] that revealed the different evolution of strain hardening in different mechanical tests (tension, compression, shear, etc.). These workers modelled this phenomenon through the specific rotation of each crystallite and each amorphous chain under the effect of accumulated strain increments. Such micromechanical theories predicted quite well the development of anisotropy in semi-crystalline polymers and reproduced the experimental stress–strain curves far better than the oversimplified von Mises approach.

Lastly at large strains, deformation damage becomes considerable and needs to be taken into account in the modelling of polymer plasticity. Although cavitation mechanisms had been observed by early workers (e.g. [23]), it is only during the last decade that this aspect has been really taken into consideration for interpreting the dependence of strain path on the density and mechanical properties of polymers [24,25]. In semi-crystalline polymers, such effects were ascribed to a series of non-cohesive mechanisms including crystal fragmentation, interspherulitic decohesion, crazing and cavitation [26,27].

Because of the failure of the simple models based on von Mises criteria, the accurate simulation of solid-state forming processes can be accomplished only if complete sets of material data are available. In particular it is essential to characterise the plastic behaviour for a variety of mechanical tests over a wide range of strain rates. The aim of this paper is to apply this strategy to the case of POM at a single testing temperature of 160 °C, which is the optimum thermoforming temperature [5] with the exception of the plane strain compression (PSC) tests. The results of the uniaxial tensile tests and simple shear tests performed at Nancy and that of PSC tests carried out at Leeds will be examined. The discussion will be devoted to the comparison of stress–strain relations obtained with these different strain paths with special attention paid to orientation and damage phenomena.

## 2. Material and experimental techniques

### 2.1. Sample preparation

The material used in this study was a commercial grade of POM, Delrin DE 7031®, from DuPont Engineering Polymers (Wilmington, Delaware, USA). The density, number average molecular weight and polydispersity of this grade are $\rho = 1.423\ \mathrm{g/cm^3}$, $\overline{M}_n = 66,000\ \mathrm{g/mol}$ and $I_p = 2.0$, respectively. The melt temperature and crystallinity of this grade, determined by DSC at a scanning rate of 10 °C/min are $T_m = 178 \pm 1$ °C and $X_c = 57 \pm 0.5$ wt%, respectively.

Rectangular plates of dimensions $200 \times 200 \times 4\ \mathrm{mm^3}$ were prepared from POM pellets in a hydraulic press at 200 °C. After compression moulding, the polymer was solidified at a slow cooling rate to ensure that the structure and morphology of the compressed plates are homogeneous both through the thickness and along the length.

### 2.2. Uniaxial tensile tests

The stress–strain behaviour of the POM was determined under uniaxial tension by means of a novel video-controlled testing system, VidéoTraction©, developed at INPL, Nancy and commercially developed by Apollor (Vandoeuvre, France). The method has been described in detail in a previous paper [28]. Consequently only its essential features will be recalled here. The tensile samples were machined from the compression moulded POM plates with a numerically driven milling machine (Charly Robot, France) in order to define

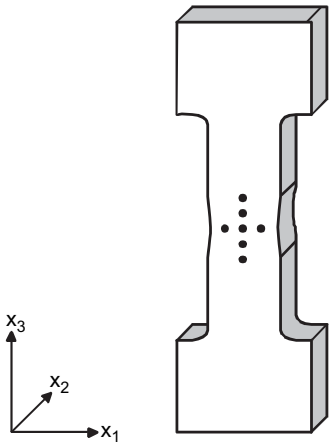


Fig. 1. Specimen for tensile tests.

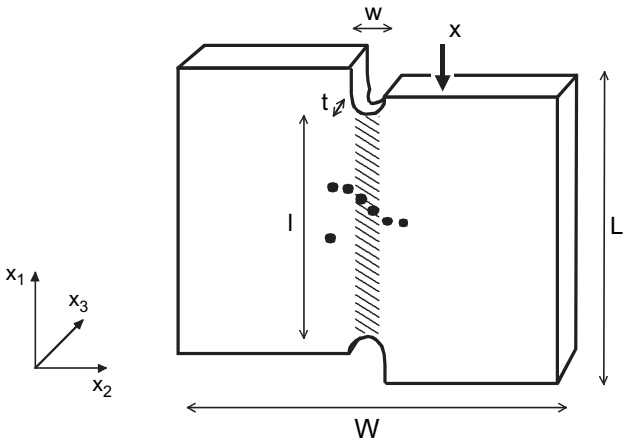


Fig. 2. Specimen for simple shear test.

a calibrated zone of dimensions, $50 \times 10 \times 4\ mm^3$ (Fig. 1). In order to force the onset of necking in the central part of the specimen, the width of the samples was locally reduced by 10% with a curvature of about 20 mm. The goal of this specimen design is to determine the plastic behaviour of the polymer in the Representative Volume Element (RVE) made up of the material slice at the narrowest cross-section, where the strain rate is maximum before and after the initiation of necking.

The principle of the method consists analysing in real time, via a computerised vision system, the coordinates ($x_1$, $x_3$) of seven markers printed prior to the test on the front face of the specimens. The true axial strain in the RVE, $\varepsilon_{33}$, was assessed by polynomial interpolation from the relative displacements of the five dots aligned along the sample axis. The transverse strain, $\varepsilon_{11}$, was also determined in the same volume element from the movements of the three markers aligned perpendicularly to the tensile axis. Providing that the deformation was transversally isotropic in the RVE (a condition that was validated by measuring the cross-section dimensions with a precision calliper before and after the test), the through-thickness strain, $\varepsilon_{22}$, was simply taken to be equal to the transverse strain, $\varepsilon_{11}$. In addition to measuring the three principal components of strain in the same material element, the Vidéo-Traction© system is capable of maintaining a constant true axial strain rate, $\dot{\varepsilon}_{33}$, during the entire tensile test by an appropriate regulation of the actuator speed of the servo-hydraulic machine (MTS 810). The true axial stress undergone locally by the material can be given directly by the load per unit actual cross-section: $\sigma_{33} = (P/S_0)\exp(-\varepsilon_{11} - \varepsilon_{22})$. Hence, the constitutive equation of the material can be readily obtained in the form: $\sigma_{33}(\varepsilon_{33}, \dot{\varepsilon}_{33})$ [28].

### 2.3. Simple shear tests

Another special testing method developed by the Nancy team was the simple shear test [29]. The original "rail shear test" principle developed in the 1980s was still utilised in the present version, but the sample geometry and the shear assessment method were recently optimised. The sample (Fig. 2) was a parallelepiped, machined from the compression moulded POM plates with overall dimensions, $L = 30$ mm and $W = 40$ mm. The specimen was subjected to macroscopic shear deformation by imposing a vertical translation, $x$, to the right part of the specimen with respect to the left part. This movement is guided by means of a high-precision ball slider.

In order to assess quantitatively the local shear behaviour of the material in a pre-determined zone and thus avoid the spreading of the deformation field, a calibrated portion was prepared in the overall parallelepiped slab. This zone was defined by a round-bottomed longitudinal groove machined on the rear face of the sample and limited in length by two round-based notches at the upper and lower ends. The plastic shear was therefore confined to a vertical band of length $l = 26$ mm, width $w = 4$ mm and minimum thickness $t = 2$ mm. If the shear field were homogeneous in the reduced portion, the imposed movement, $x$, would produce a simple shear strain $\gamma = x/w$. However, since the sheared zone was limited (in length and in thickness) by rounded surfaces, the application of this definition of shear strain would lead to overestimated measurements. For this reason a special version of the video-controlled testing technique (VidéoShear©) was developed to assess quantitatively the local shear strain in the median plane of the calibrated band. In brief, a series of six contrasting dots were printed on its flat front face originally aligned along the horizontal axis $x_2$, plus an extra dot was printed at a distance of about 6 mm below the left dot of the horizontal row. Since the movements of the dots were recorded by the video extensometer, the maximum slope of the polynomial curve describing the vertical displacement of the six dots gave access to the local shear strain $\gamma$ in the centre of the specimen. The aim of the seventh dot was to correct, if necessary, the shear slope defined above by the rotation that would result from the overall slippage of the specimen in the grips (actually, it was found here that this rotation was negligible). Also the local shear stress was accessible via this technique due to the fact that simple shear did not significantly affect the vertical cross-section in the calibrated zone.

Consequently, the shear stress can be directly obtained from the applied load, $P$, by the relation $\tau = P/(l \times t)$.

### 2.4. Plane strain compression tests

The experimental setup for plane strain compression (PSC) tests is shown in Fig. 3. In this test the sample was a parallelepiped and was compressed between two rectangular dies. The material initially involved in the compression was defined by the breadth of the plate, $b_0 = 60$ mm, thickness, $h_0 = 4$ mm and the width of the dies, $w = 14$ mm. The highly polished die faces were lubricated with molybdenum disulphide grease to minimise the friction with the sample during the test. This lubricant has been shown to be ideal for compression tests on aluminium alloys [30]. The sample was heated to the desired temperature for 60 min before testing, and maintained at that temperature with two regulated cartridge heaters. Edge insulation was provided with the aid of resin blocks on both the sides of the samples to minimise temperature gradients in the sample along its width and thickness. The PSC tests applied here corresponded to the protocols described in the test guide issued by the National Physical Laboratory [31].

Because no constraint was applied to the specimen at the end of the compression zone in the PSC test, there was a longitudinal spread of the sample in the tools, so that the contact area between the tools and sample increased during the test. The ''instantaneous'' breadth, $b$, cannot be measured directly during the test because the software controlling the Instron testing machine only delivers the relative distance, $h$, of the dies. Consequently, $b$ was determined from an empirical relationship [32], $b = b_0\{1 + C[1 - (h/h_0)^n]\}$ where $b_0$ and $h_0$ are the initial breadth and thickness of the specimen, respectively, while $n$ and $C$ are the adjustable parameters relevant for the material − tool system under investigation. The value of the exponent $n$ in the above equation was chosen *a priori* as equal to 0.18, as in previous tests for aluminium alloys [33] and the ''spread coefficient'', $C$, was determined from the sample dimensions measured before and after the tests. As shown previously [33], the Hencky strain undergone by the material in the PSC test can be given by the relation $\varepsilon = f \ln(h/h_0)$, where $f$ is a correction factor which expresses the ratio of the strain in this test with respect to the strain in purely uniaxial compression. The correction factor is given by: $f = b/\left[b - w + \left(\sqrt{3}w/2\right)\right]$.

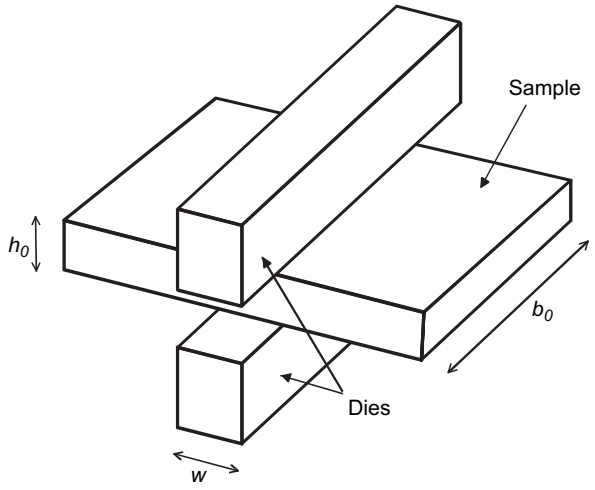


Fig. 3. Plane strain compression tests.

The PSC tests in this work were performed at five predefined crosshead speeds of the testing machine, which correspond to five nominal strain rates, $\mathrm{d}(h_0/h)/\mathrm{d}t$, ranging from $10^{-4}$ to $1\ \mathrm{s}^{-1}$. However, a constant rate of compression did not correspond to a constant rate of Hencky strain at large deformation, because of its logarithmic form. The prescribed strain rate was correct only at the beginning of the test, and then it increased gradually as the thickness of the specimen decreased between the dies. Consequently, in order to make the presentation of results more coherent, the test results were post-processed and the stress–strain curves were reconstructed at constant true strain rate. This treatment was simply based on the stress interpolation for each value of the applied strain.

The friction between the sample and the die faces was not accounted for in the true stress–strain calculations because the friction coefficient was likely to be very low (<0.1) between the POM sample and the steel dies. Consequently, the true flow stress was simply calculated as the load per actual cross-section of the compressed zone: $\sigma = P/(w \times b)$.

### 2.5. Determination of volume effects in the different loading conditions

As pointed out in Section 1, one aim of this work was to analyse the damage processes for the three strain paths selected. However, the specific constraints associated with the three test geometries did not give access, with an equal simplicity, to the volume changes. This was the reason why different experimental techniques were adopted for the tensile, shear and plane strain compression tests.

For the tensile tests, the VidéoTraction© system had the unique feature to give access in real time to the three principal strains in the RVE: $\varepsilon_{11}$, $\varepsilon_{22}$ and $\varepsilon_{33}$. Consequently, by the virtue of the local symmetry of the strain field in the centre of the specimen, the Hencky volume strain $\varepsilon_v = \varepsilon_{11} + \varepsilon_{22} + \varepsilon_{33} = \ln(V/V_0)$ was directly obtained at the RVE whose initial volume, $V_0$, changes to a different value, $V$ under strain. The efficiency of this procedure was checked carefully for a number of different polymers in a recent publication [34], which showed that the accuracy of the $\varepsilon_v$ measurements was better than $10^{-2}$.

For the shear and plane strain compression tests, the volume strain was not directly accessible from the operational data provided by the testing machine. However, it should be appreciated from the assumptions introduced in Sections 2.2 and 2.3 to determine strain and/or stress that volume strain effects were expected to be small in the material for these strain paths. For this reason a different approach was adopted based on the physical analysis of density variations in the deformed material. This could have been done by means of the classical flotation method, but in this work, an alternative technique

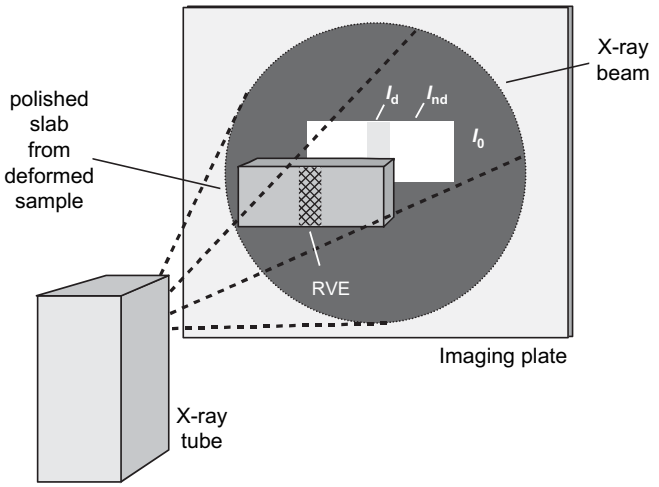


Fig. 4. Quantitative X-ray densitometry.

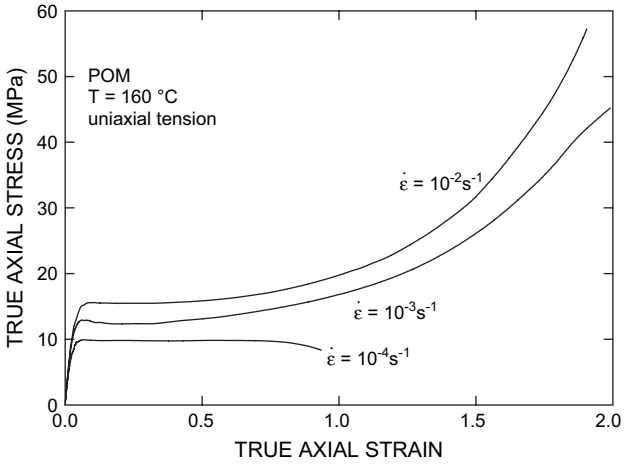


Fig. 5. Stress–strain behaviour of POM under uniaxial tension at $T = 160\ ^\circ C$ for different strain rates.

based on X-ray densitometry was employed in order to avoid the artefacts possibly caused by cutting small bits of polymer from inside the deformed RVE and immersing them in the reference liquid.

The technique (Fig. 4) utilised here is simple and has been described earlier [35], so only its main features are recalled here. A slab of uniform thickness was carefully cut and polished out of each sample deformed in simple shear or in plane strain compression. Since deformation is not homogeneous in either technique, the interest was focused at the location of the RVE. The slab was attached onto an imaging plate (FujiFilm) sensitive to the X-ray beam emitted by a filtered tungsten tube. After irradiating the specimen with X-rays for a short prescribed time (about 10 s), the specimen was detached from the imaging plate and the distribution of transmitted intensity was quantitatively analysed with a special electronic photometer with a resolution of 50 μm (FujiFilm BAS 5000). Three relevant levels of intensities were measured: (i) the background intensity, $I_o$, outside the shadow of the sample, (ii) the ''non-deformed'' intensity, $I_{nd}$, at specimen zones unaffected by the applied strain field, and (iii) the ''deformed'' intensity, $I_d$ corresponding to the location of the RVE. The classical Beer–Lambert's law states that the transmitted intensity is given by $I = I_0 \exp(-\mu \times t)$, where $t$ is the uniform thickness of the slab and $\mu$ the local through-thickness absorption coefficient at each point of slab, which is related in turn to the local density. Since plastic damage produces a local density reduction, the local volume strain can be readily obtained through the relation $\varepsilon_v = \ln(\rho_{nd}/\rho_d) = \ln[\ln(I_0/I_{nd})] - \ln[\ln(I_0/I_d)]$ following the notations introduced above. The resolution of this method is of the order of 1%.

## 3. Experimental results

### 3.1. Typical stress–strain behaviour under various deformation modes

The axial stress vs. axial strain curves shown in Fig. 5 were obtained under uniaxial tension at 160 °C for different strain rates $\dot{\varepsilon}_{33}$ ranging from $10^{-4}$ to $10^{-2}\ s^{-1}$. The reproducibility of each curve was checked by three tests performed under the same conditions. This graph is therefore typical of the behaviour of POM at elevated temperature. Several interesting features deserve attention. First, all experiments showed the same deformation stages including short visco-elastic behaviour at strains lower than about 0.06, followed by a rounded yield point. After yielding, the curves show a very long plastic regime that extended until rupture occurs in the RVE at large accumulated strains between 0.8 and 2.0 depending on the strain rate. These Hencky strains at rupture corresponded to local extension ratios, $\lambda$, between 2.2 and 7.4. Apart from the specific cases of specimens deformed at the slowest strain rate, the tests revealed progressively increasing strain hardening in the plastic deformation stage, the curve showing a progressive upturn that raised the tensile stress to a level about three times the plastic threshold at yield. Also it is evident, as for many other semi-crystalline polymers at elevated temperature [36], that the strain rate sensitivity of POM was considerable, a one decade upward shift in strain rate produced a flow stress increase of about 5 MPa.

Fig. 6 shows the stress–strain behaviour of POM at the same temperature as above ($T = 160\ ^\circ C$), but now under simple shear. The selected shear strain rates were chosen in such a way that they were equivalent (following the von Mises criterion) to the axial strain rates adopted in tension [29] (see Section 4.2 below for discussion). The stress–strain curves exhibited the same general tendencies with an initial visco-elastic range followed, after a round yield point, by a long plastic stage. Qualitatively, the influence of strain rate is still important. The main difference between the curves recorded in tension and in shear concerns the amount of plastic strain hardening. As previously observed for various semi-crystalline polymers [24], plastic flow in shear proceeded at nearly constant stress. As such, POM behaved under shear at elevated temperature like an elastic perfectly plastic material.

Fig. 7 shows the corresponding behaviour of POM under plane strain compression at the same temperature of 160 °C over a similar range of strain rates but going up to $1\ s^{-1}$. All

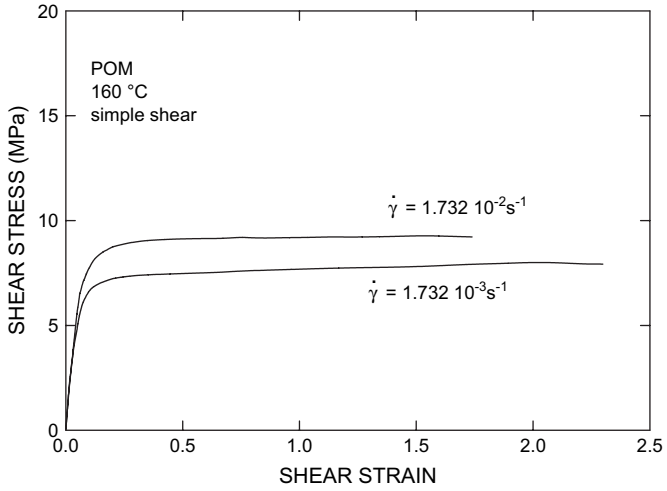


Fig. 6. Stress–strain behaviour of POM under simple shear at $T = 160\,^{\circ}C$ for different strain rates.

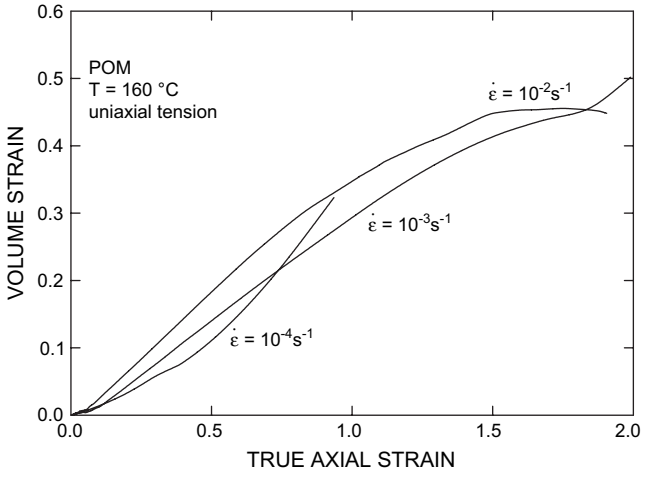


Fig. 8. Evolution of volume strain under uniaxial tension at $T = 160\,^{\circ}C$ for different strain rates.

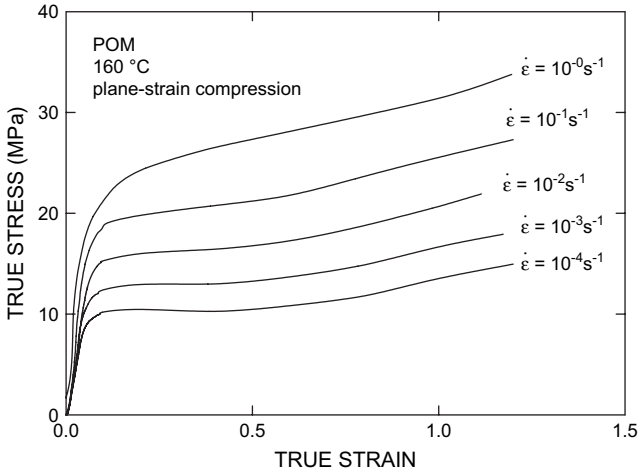


Fig. 7. Stress–strain behaviour of POM under plane strain compression at $T = 160\,^{\circ}C$ for different strain rates.

the features common to tension and shear are again found here. However, it can be observed that the curves showed a fairly constant positive slope in the plastic stage at large strains. Similar observations were made at other temperatures, although of different magnitudes. This contrasted with the zero slope measured in shear and the gradually increasing slope recorded in uniaxial tension.

### 3.2. Assessment of deformation damage

As indicated earlier, plastic damage was easy to characterise under tension because the VidéoTraction© system provides the evolution of volume strain in real time during the tensile test. Fig. 8 shows this information for the three strain rates at 160 °C and proves the importance of damage mechanisms during the tensile plastic deformation of POM at elevated temperature. This was expected since extensive sample whitening was observed by the naked eye during the course of the tensile tests. Such whitening is a very common feature for most semi-crystalline polymers subjected to stretching, although it has been largely ignored by most of the authors. Since the overall volume change was measured quantitatively, several important points can be made: (i) dilation is a very early process in the deformation of POM since volume strain increases as soon as the yield point is passed, (ii) the rate of damage is nearly steady since the slope of the $\varepsilon_v$ vs. $\varepsilon_{33}$ curve does not saturate significantly before the end of the tests, (iii) Hencky volume strain reaches values close to 0.5 at rupture, which represent a volume increase as high as 65%, (iv) the intensity of volume strain does not seem to be much influenced by strain rate, at least in this example. At this point of the investigation, it can be concluded unambiguously that damage mechanisms play an essential role in the plastic deformation of POM under uniaxial tension at elevated temperature, because the amount of volume strain represents a significant fraction of the tensile strain.

In order to confirm the above results obtained from the macroscopic dilation in a different way, the X-ray densitometry technique was applied to specimens that had been subjected to prescribed levels of strain in uniaxial tension and subsequently cooled to ambient temperature. The radiographic image displayed in Fig. 9 actually shows considerable increase of transmitted X-ray intensity in the necked part of the sample. This quantitative effect is obviously ascribed to the development of extensive cavitation in the centre of the neck where plastic deformation has concentrated the deformation. Also, apart from the general intensity gradient, it is interesting to remark that local defects are observed which appear as darker bands inclined at about 45° to the tensile direction. The development of cavitation bands along the planes of maximum shear during the plastic deformation of solid polymer has been already acknowledged [37] in the literature and their detailed mechanisms will be the subject of a forthcoming paper.

The X-ray densitometry images were obtained with the sheared and plane strain compressed samples. It was remarkable at first sight that no contrast was visible in the deformed zone. Detailed photometric analysis of the electronic images

Fig. 9. X-ray radiography of a POM sample deformed in uniaxial tension at 160 °C with a strain rate of $10^{-3}\,s^{-1}$ (the maximum true strain was $\varepsilon_{33} = 1.2$).

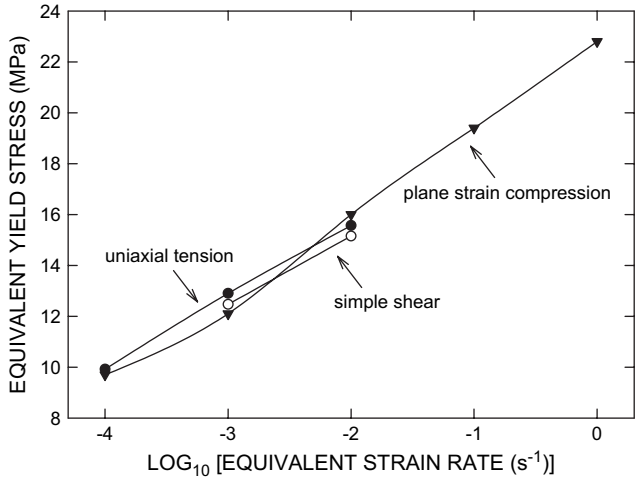


Fig. 10. Influence of equivalent strain rate on equivalent yield stress for the three testing methods at 160 °C.

was performed which actually proved that no significant change of density (hence no significant volume strain) occurs either in simple shear or in PSC. It is interesting to note that complementary investigations performed on POM samples deformed at 160 °C with complex strain paths (to be published later) showing that the occurrence of damage is intimately connected to the existence of a positive hydrostatic stress.

## 4. Discussion

### *4.1. Influence of temperature and strain rate on yield stress*

First the effect of temperature and strain rate on the yield process will be discussed. Because no stress drop was recorded in either test, the yield stress cannot be defined as usual from a local maximum in the stress–strain curves. Instead, the plastic threshold was defined by the intersection of lines extrapolated from the visco-elastic and plastic ranges, respectively. Also, the yield stresses in shear were transformed into the von Mises equivalent yield stress, as explained in Section 4.2 below, giving the results summarised in Fig. 10, which compares the evolution of equivalent yield stress with equivalent strain rate for the three testing techniques at 160 °C. First, it can be seen that the strain rate sensitivity of POM is quite uniform, the slope of the yield stress vs. ln(strain rate) being nearly constant over four decades. Secondly these results showed that the activation of plastic mechanisms at elevated temperature is very dependent on time, since the slope of the curve is very steep. Thirdly it can be seen that the von Mises yield criterion is a good candidate to describe the yield process since the equivalent stress data arising from the three tests employed are quite accurately superimposed.

The temperature and the strain rate dependence of the yield behaviour can be represented by the Eyring equation for a thermally activated rate process [38],

$$\dot{\varepsilon} = \dot{\varepsilon}_0 \exp\left(\frac{-\Delta H}{kT}\right)\sinh\left(\frac{v\sigma}{kT}\right) \tag{1}$$

where $\dot{\varepsilon}$ is the strain rate, $\dot{\varepsilon}_0$ is the pre-exponential factor, $\Delta H$ is the activation energy, $k$ is the Boltzmann constant, $T$ is the temperature, $v$ is the activation volume for the molecular event and $\sigma$ is the applied stress. For high values of stress, Eq. (1) reduces to:

$$\dot{\varepsilon} = \frac{\dot{\varepsilon}_0}{2}\exp\left[\frac{-\Delta H + v\sigma}{kT}\right] \tag{2}$$

which can be rearranged to give the following:

$$\frac{\sigma}{T} = \frac{\Delta H}{vT} + \left(\frac{k}{v}\right)\ln\left(\frac{2\dot{\varepsilon}}{\dot{\varepsilon}_0}\right) \tag{3}$$

Eq. (3) indicates that the plot of yield stress against logarithmic strain rate at constant temperature should produce a straight line. The yield stress of POM in PSC was fitted to an Eyring equation as described by Eq. (3) and the results are shown in Fig. 11. It can be seen that the Eyring theory can be successfully used to describe the yielding behaviour in POM at elevated temperatures.

Activation volumes and activation energies were obtained on the basis of Eq. (3) and the results are summarised in Table 1 along with the values of the yield stress. The activation volume increases with temperature from 1.5 $nm^3$ at 120 °C to 6.28 $nm^3$ at 165 °C, which is of the same order of magnitude as the activation volume for other polymers in the literature [19,39–42]. The activation energy is in the range 11.6–14.4 kcal/mol which would be consistent with a localised slip process as expected for a crystalline $\alpha$ relaxation. Literature values of 19.3 kcal/mol for $\alpha$ relaxation have been quoted at lower temperatures based on dielectric relaxation measurements [43].

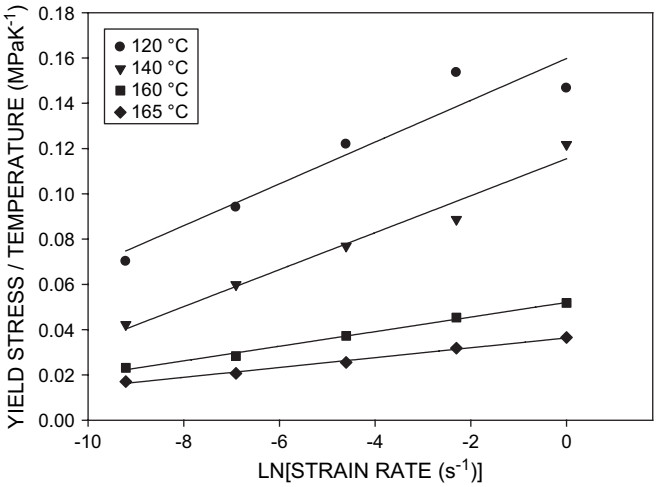


Fig. 11. Ratio of the yield stress in compression to temperature as a function of logarithmic strain rate according to the Eyring equation for POM.

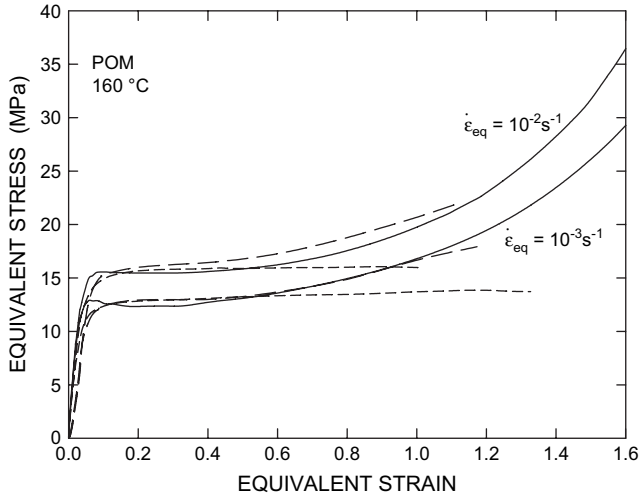


Fig. 12. Comparison of the "equivalent" stress–strain behaviour for the three strain paths at 160 °C. Solid lines = uniaxial tension, long dashed lines = plane strain compression, short dashed lines = simple shear.

Table 1
Eyring parameters for yield in compression

| Temperature, K | Activation volume, $nm^3$ | Activation energy, kcal/mol |
|---|---|---|
| 393 | 1.50 | 13.6 |
| 413 | 1.68 | 11.6 |
| 433 | 4.31 | 13.9 |
| 438 | 6.28 | 14.4 |

### 4.2. Comparison of material behaviour for different strain paths

Particular mention should be made here of the notion of so-called "equivalent" stress and strain in simple shear. The problem of predicting behaviour under generalised strain paths was among the core questions of this work, so that none of the classical yield criteria is better than others *a priori*. Nevertheless, it was decided to transform systematically the mechanical variables provided by the shear tests ($\gamma$, $\dot{\gamma}$ and $\tau$) into their equivalent counterparts in the spirit of von Mises: $\varepsilon_{eq} = \gamma/\sqrt{3}$, $\dot{\varepsilon}_{eq} = \dot{\gamma}/\sqrt{3}$ and $\sigma_{eq} = \tau \times \sqrt{3}$ [44]. This strategy has two advantages. First, it makes the manipulation of the experimental data coming from the different tests more convenient and secondly it provides a good tool to check the intrinsic validity of the von Mises criterion.

Following the above procedure, the corresponding evolutions of equivalent stress vs. equivalent strain at two equivalent strain rates ($\dot{\varepsilon}_{eq} = 10^{-3}\ s^{-1}$ and $\dot{\varepsilon}_{eq} = 10^{-2}\ s^{-1}$) are plotted in Fig. 12 for the three testing methods.

As noticed before, the yield point at a given strain rate is nearly the same for the three strain paths. In view of much previous evidence for the pressure dependence of the yield stress in polymers [38], it is surprising that the present results for POM do not show any effect of the hydrostatic component of stress. This point will need to be critically investigated in further work.

In contrast, the curves separate at large strains. The most important difference concerns the stress evolution under simple shear that levels off rapidly, whereas the curves for tension and compression show significant plastic hardening. As stated before for other thermoplastic polymers [22,24], the easy plastic flow of POM under shear is mainly due to the progressive tilt of the crystallites in such a way that macromolecular chains become aligned with the shear direction. Since "chain slip" is the most favourable deformation mode in the crystal phase, one readily figures out that the average Schmid's factor of active slip systems decreases gradually with applied strain. Actually, it is noted that the curves under simple shear do exhibit only a very gradual softening. According to Refs. [22,24], the small amplitude of this softening probably results from the hardening contribution of the rubber-like amorphous phase that increases its resistance to shear as deformation increases.

Concerning the curves obtained from tests under uniaxial tension and plane strain compression, Fig. 12 shows that the responses for these two deformation modes are nearly undistinguishable in terms of equivalent stress–strain curves in the range of moderate strains ($\varepsilon_{eq} < 1.2$). Although this result is reasonable as long as chain orientation is small, the strain hardening under tension should be higher than under PSC at large strains since experimental data and modelling previously published in the case of polyethylene at room temperature [45] showed that the anisotropy of the microstructural texture induced by plastic deformation is more pronounced under tension than under PSC. This is because the two principal strains become negative under uniaxial tension while one remains at zero under PSC. Not only do our results not verify this tendency but the equivalent stress–strain curve under tension even lags below the compression curve at high strain rate. This apparent discrepancy is explained by the following arguments.

As demonstrated in Section 3.2, POM undergoes very different amounts of plastic damage according to the strain path followed. Unlike uniaxial tension that provokes dramatic volume strain (initiating right at the yield point and increasing

up to $\varepsilon_v \approx 0.5$ before rupture), PSC keeps the polymer intact from cavitation. It is obvious that these contrasting phenomena result from the difference in hydrostatic stress: positive in tension and negative in compression. Consequently, it is likely that the limited plastic hardening in tension results from the microstructural weakening due to micro-porosity. This phenomenon has already been discussed by Lemaitre [46] for damage in metals. The macroscopic stress supported by the tensile specimens undergoing plastic damage is lower than the stress in the solid fraction of the material. The latter is termed as the ''intrinsic axial stress'', and denoted as: $\sigma^i_{33}$. In a mean-field approach, the intrinsic stress can be simply calculated as the applied load divided by the average cross-section of the solid ligaments between the voids. Since in a material with evenly distributed cavitation, the volume void fraction is equal to the surface void fraction [47], one readily finds that $\sigma^i_{33} = \sigma_{33} \exp(\varepsilon_v)$. As for the ''intrinsic axial strain'', it also represents the average strain in the solid material between the voids. Hence, as a first approximation, it is simply equal to the macroscopic strain.

The ''intrinsic'' stress–strain curves obtained via the above transformation of the tensile data are displayed in Fig. 13 with the same scales as in Fig. 12. It is evident in this graph that the hardening of the solid polymeric ligaments, Fig. 13, is higher in uniaxial tension than the hardening of the cavitated material, Fig. 12. The stress–strain curves are now compared for the different strain paths more legitimately since the three sets of stress–strain curves (in tension, PSC and simple shear) refer to the proper response of the solid polymer itself, without the perturbation of the cavitation. On this basis, it is observed that the tensile behaviour is clearly distinguished from the behaviour under PSC, as expected from the micromechanical models. A detailed discussion of the intrinsic behaviour of polymers is presently in the course of implementation at Nancy for a variety of materials and will be the object of forthcoming publications.

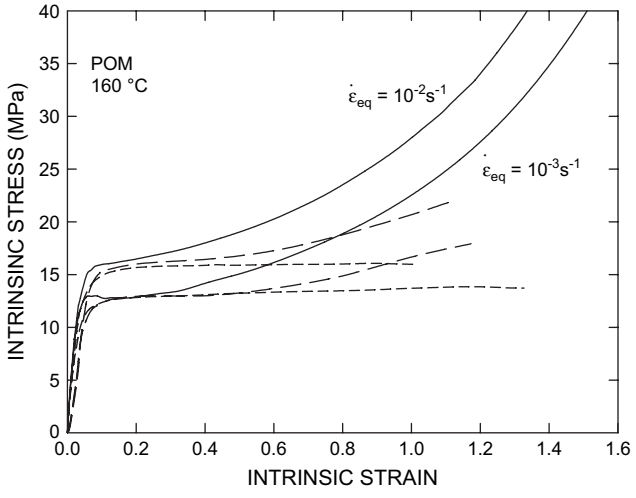


Fig. 13. Comparison of the ''intrinsic'' stress–strain behaviour for the three strain paths at 160 °C. Solid lines = uniaxial tension, long dashed lines = plane strain compression, short dashed lines = simple shear.

## 5. Conclusions

It is apparent from the results of the careful tension, shear and compression tests described in this paper that the inelastic mechanical behaviour of POM at elevated temperature is a complex function of state of stress, strain rate and the internal damage mechanisms that occurred in the semi-crystalline polymer. At low plastic strains, the equivalent yield stress was a linear function of the logarithmic equivalent strain rate for all loading conditions, suggesting an Eyring-type relation with a high activation volume. Differences in the yield stress in tension, compression and shear were relatively minor. In tension only, finite volumetric strain due to microvoiding occurs immediately post-yield and increased to around a Hencky volumetric strain of approximately 0.5 at the time of fracture. Precise measurements of this volumetric strain allowed the true tensile stress–strain curves for the solid polymer to be obtained. The large differences between this curve and the corresponding equivalent stress–strain curves in compression and in shear at high strains were due to the evolution of texture (orientation hardening), which was facilitated by uniaxial tensile loading. However, at low strains, less than about 0.2, the fact that the flow stresses for the three strain paths are virtually identical indicates that the von Mises relations are appropriate provided allowance is made for volume dilation due to void growth.

## References

[1] Ward IM, Taraiya AK, Coates PD. Solid state extrusion and die drawing. In: Hyun KS, editor. Solid phase processing of polymers. Munich: Hanser; 2000. p. 328–65.
[2] Coates PD, Ward IM. Journal of Polymer Science Part B: Polymer Physics 1978;16(11):2031–47.
[3] Coates PD, Ward IM. Polymer 1979;20(12):1553–60.
[4] Gibson AG, Ward IM. Journal of Materials Science 1980;15(4):979–86.
[5] Taraiya AK, Mirza MS, Mohanraj J, Barton DC, Ward IM. Journal of Applied Polymer Science 2003;88(5):1268–78.
[6] Gibson AG, Ward IM. Journal of Polymer Science Part B: Polymer Physics 1978;16(11):2015–30.
[7] Powell AK, Craggs G, Ward IM. Journal of Materials Science 1990; 25(9):3990–4000.
[8] Nakayama K, Kaito A. Kobunshi Ronbunshu 1991;48(11):679–84.
[9] Chaffey CE, Taraiya AK, Ward IM. Polymer Engineering and Science 1997;37(11):1774–84.
[10] Ajji A, Cole KC, Dumoulin MM, Ward IM. Polymer Engineering and Science 1997;37(11):1801–8.
[11] Morawiec J, Bartczak Z, Kazmierczak T, Galeski A. Materials Science and Engineering A: Structural Materials Properties Microstructure and Processing 2001;317(1–2):21–7.
[12] Bartczak Z, Morawiec J, Galeski A. Journal of Applied Polymer Science 2002;86(6):1413–25.
[13] Coates PD, Gibson AG, Ward IM. Journal of Materials Science 1980; 15(2):359–75.
[14] Mirza MS, Taraiya AK, Ward IM, Barton DC. Proceedings of the Institution of Mechanical Engineers Part E: Journal of Process Mechanical Engineering 2003;217(E2):123–31.
[15] Peterlin A. Journal of Materials Science 1971;6(6):490–508.
[16] Lin L, Argon AS. Journal of Materials Science 1994;29(2):294–323.
[17] Mears DR, Pae KD, Sauer JA. Journal of Applied Physics 1969;40(11): 4229–37.

[18] Rabinowitz S, Ward IM, Parry JSC. Journal of Materials Science 1970; 5(1):29–39.
[19] Davis LA, Pampillo CA. Journal of Applied Physics 1971;42(12):4659–66.
[20] Motashar FA, Unwin AP, Craggs G, Ward IM. Polymer Engineering and Science 1993;33(19):1288–98.
[21] Parks DM, Ahzi S. Journal of the Mechanics and Physics of Solids 1990;38(5):701–24.
[22] Dahoun A, Canova GR, Molinari A, Philippe MJ, Gsell C. Textures and Microstructures 1991;(14–18):347–54.
[23] Hay IL, Keller A. Journal of Materials Science 1967;2(6):538–58.
[24] Gsell C, Dahoun A. Materials Science and Engineering A: Structural Materials Properties Microstructure and Processing 1994;175(1–2): 183–99.
[25] Komatsu T, Enoki S, Aoshima A. Polymer 1991;32(11):1988–93.
[26] O'Leary K, Geil PH. Journal of Macromolecular Science – Physics 1968;B2(2):261–300.
[27] Butler MF, Donald AM, Ryan AJ. Polymer 1998;39(1):39–52.
[28] G'Sell C, Hiver JM, Dahoun A. International Journal of Solids and Structures 2002;39(13–14):3857–72.
[29] Gsell C, Boni S, Shrivastava S. Journal of Materials Science 1983; 18(3):903–18.
[30] Maurice C, Piot D, Klocker H, Driver JH. Metallurgical and Materials Transactions A: Physical Metallurgy and Materials Science 2005; 36A(4):1039–47.
[31] Lacey AJ, Loveday MS, Mahon GJ, Roebuck B, Sellars CM, van der Winden MR. Measuring flow stress in hot plane strain compression tests. In: Measurement good practice, vol. 27. Teddington: National Physical Laboratory; 2002. pp. 1–85.
[32] Mirza MS, Sellars CM. Materials Science and Technology 2001;17(9): 1142–8.
[33] Silk NJ, van der Winden MR. Materials Science and Technology 1999;15(3):295–300.
[34] G'Sell C, Bai SL, Hiver JM. Polymer 2004;45(17):5785–92.
[35] Rezgui F, Swistek M, Hiver JM, G'Sell C, Sadoun T. Polymer 2005; 46(18):7370–85.
[36] Duffo P, Monasse B, Haudin JM, Gsell C, Dahoun A. Journal of Materials Science 1995;30(3):701–11.
[37] Bucknall CB. Journal of Microscopy – Oxford 2001;201(2):221–9.
[38] Ward IM. Mechanical properties of solid polymers. London: Wiley-Interscience; 1971.
[39] Ward IM. Journal of Materials Science 1971;6(11):1397–417.
[40] Hamdan S, Swallowe GM. Journal of Materials Science 1996;31(6): 1415–23.
[41] Alberola ND, Mele P, Bas C. Journal of Applied Polymer Science 1997;64(6):1053–9.
[42] Zhou YX, Mallick PK. Polymer Engineering and Science 2002; 42(12):2449–60.
[43] Read BE, Williams G. Polymer 1961;2(3):239–55.
[44] Canova GR, Shrivastava S, Jonas JJ, G'Sell C. In: Newby JR, Niemeier BA, editors. Formability of metallic materials–2000 AD, vol. ASTM STP 753. American Society for Testing Materials; 1982. p. 189–210.
[45] Lee BJ, Argon AS, Parks DM, Ahzi S, Bartczak Z. Polymer 1993; 34(17):3555–75.
[46] Lemaitre J. A course on damage mechanics. New York: Springer-Verlag; 1996.
[47] Delesse A. Annales des Mines 1848;13:379–88.